Check for updates

Interconversion between multicomponent slider-on-deck and palladium capsule: regulation of catalysis and encapsulation†

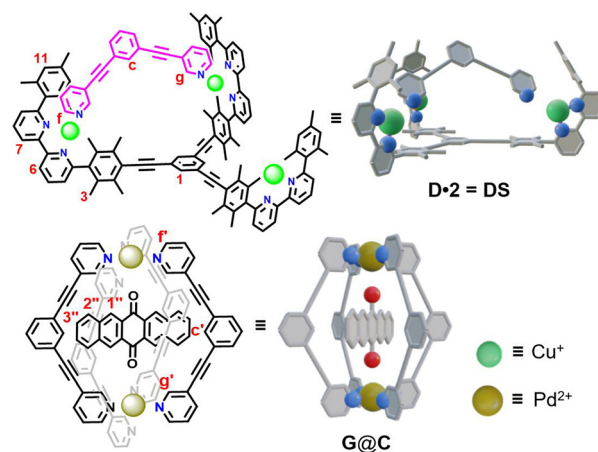Isa Valiyev, [ID] Indrajit Paul, Yi-Fan Li, Emad Elramadi [ID] and Michael Schmittel [ID] *

When the slider-on-deck $[Cu_3(1)(2)]^{3+}$ and guest G were treated with palladium(II) ions, the biped **2** was released from $[Cu_3(1)(2)]^{3+}$ generating the nanocage $[Pd_2(2)_4(G)]^{4+}$ with guest G being encapsulated (NetState-II). This transformation that was reversed by the addition of DMAP enabled modulation of both the overall fluorescence and the activity of copper(I) catalyzing an aza Hopf cyclization.

Over the years, researchers have investigated methods to mimic complex multicomponent catalysts found in nature, such as ATP synthase,[1] by manmade prototypes that bring together catalysis, host–guest chemistry,[2] and dynamic molecular motion.[3] All these elements are combined in slider-on-deck machinery[4] with either on/off or up/down regulation of catalysis.[5] Since nanoscale metallocages are well established in sensing,[6] catalysis,[7] and highly selective binding,[8] interconnecting dynamic molecular machines and functional nanocages may offer new venues for functional applications.

Herein, we demonstrate (i) the fully reversible interconversion of a molecular slider-on-deck and a palladium(II) capsule[9] enabling (ii) a copper(I)-based catalytic cyclization and (iii) parallel guest encapsulation. The design was based on two well-defined networked states (NetStates). NetState-I encompasses pentacene-6,13-dione as a prospective guest (**G**) and the three-component slider-on-deck **DS** (= $[Cu_3(1)(2)]^{3+}$), prepared from deck **1**, the sliding biped **2**, and copper(I) ions (1 : 1 : 3) (Scheme 1). Addition of the correct stoichiometric amount of Pd^{2+} ions afforded NetState-II involving the copper-loaded deck $[Cu_3(1)]^{3+}$ and the guest-filled palladium(II) capsule **G@C** (= $[Pd_2(2)_4(G)]^{4+}$). Notably, both networked states were catalytically active, however, at distinct reaction rates.

The design of the slider-on-deck ⇌ cage interconversion has been inspired by recent progress in chemically networked slider-on-decks,[10] nanorotors,[3c] and coordination capsules.[9,11] The required deck **1** was synthesized *via* several successive Suzuki and Sonogashira coupling reactions. Ligand **2** is a literature-known compound.[12] The stator's bipyridine stations and the biped's nitrogen-terminated feet were connected *via* copper(I) ion, *i.e.*, by HETPYP complexation.[10b] The bipyridine unit in the deck was required instead of the frequently used phenanthroline core[10,13] owing to a higher catalytic activity of the Cu^+ bound bipyridine in the aza Hopf[14] cyclization. Moreover, self-sorting between the analogous phenanthroline deck, Cu^+, and Pd^{2+} was not clean. Ligand **2** has been selected because of its ability to form both a slider-on-deck system with the Cu^+-loaded deck $[Cu_3(1)]^{3+}$ and a stable coordination capsule (**C**) with Pd^{2+} ions.

Upon addition of copper(I) ions to a mixture of ligands **1** and **2** (3 : 1 : 1), clean formation of the slider-on-deck $[Cu_3(1)(2)]^{3+}$ was observed. The multicomponent assembly was

Center of Micro and Nanochemistry and (Bio)Technology, Organische Chemie I, School of Science and Engineering, Universität Siegen, Adolf-Reichwein-Str. 2, D-57068 Siegen, Germany. E-mail: schmittel@chemie.uni-siegen.de

†Electronic supplementary information (ESI) available: Experimental procedures, compound characterizations, spectral data, UV-vis titrations data. See DOI: https://doi.org/10.1039/d3dt04300b

Scheme 1 Molecular structures and cartoon representations of main complexes.

characterized by ^{1}H-NMR (ESI,† page S5–6) and ESI-MS proving the presence of complex $[Cu_3(\mathbf{1})(\mathbf{2})]^{3+}$ by peaks at $m/z =$ 611.4 (triply charged) and $m/z = 989.4$ (doubly charged) (ESI, Fig. S27†). In addition, a single set of ^{1}H-DOSY signals ($D =$ 5.69×10^{-10} m^2 s^{-1}, $r = 9.28$ Å, in CD$_2$Cl$_2$) corroborated the clean formation of the slider-on-deck (ESI, Fig. S14†).

To investigate the dynamic behavior of the slider-on-deck, we analyzed the signal of proton 3-H by variable temperature (VT) ^{1}H-NMR in the range from 25 to −75 °C in CD$_2$Cl$_2$ (Fig. 1a). At 25 °C the proton appeared as a sharp singlet at 2.47 ppm. At *ca.* −25 °C the signal started to broaden and with further lowering of the temperature, the proton signal started to split from a singlet into two singlets. At −75 °C it separated into two singlets (1 : 2) at 2.51 and 2.37 ppm. The singlet at 2.37 ppm was assigned to the two copper(ı)-loaded bipyridine stations that are connected to the pyridine terminals of biped **2**, whereas the unloaded $[Cu(bipyAr_2)]^+$ station showed up at 2.51 ppm. The exchange frequency was determined using WinD-NMR[15] to $k_{25} = 80$ kHz at 25 °C. Activation data are displayed in Fig. 1b.

Upon addition of 0.5 equiv. of $[Pd(CH_3CN)_4](BF_4)_2$ to the slider-on-deck **DS**, the ^{1}H NMR (Fig. 2) indicated complete dissociation of biped **2** from the copper-loaded deck and clean formation of $\mathbf{C} = [Pd_2(\mathbf{2})_4]^{4+}$, a Pd$_2L_4$-type coordination capsule reported earlier by Hooley and co-workers,[12] and of $[Cu_3(\mathbf{1})]^{3+}$. The loss of biped **2** from the slider-on-deck was readily derived from the ^{1}H-NMR data, as *e.g.* proton signals 11-H and 1-H of $[Cu_3(\mathbf{1})(\mathbf{2})]^{3+}$ shifted from 6.83 and 7.55 ppm to 6.97 and 7.73 ppm, respectively, as in independently prepared $[Cu_3(\mathbf{1})]^{3+}$. The association of Pd^{2+} to **2** was readily monitored by the appearance of new peaks for f′-H, and g′-H at 9.34 and 9.50 ppm as well as the disappearance of f-H and g-H from 6.46 and 7.71 ppm, respectively. The ESI-MS proved parallel presence of complex $[Cu_3(\mathbf{1})]^{3+}$ by peaks at $m/z = 518.2$ (triply charged) and $m/z = 849.8$ (doubly charged) (ESI, Fig. S26†) and of cage $[Pd_2(\mathbf{2})_4]^{4+}$ by peaks at $m/z = 333.5$ (quadruply charged) and $m/z = 473.9$ (triply charged) (ESI, Fig. S28†).

Upon addition of two equiv. of DMAP to NetState-II (= cage **C** and copper(ı)-loaded deck $[Cu_3(\mathbf{1})]^{3+}$), clean regeneration of the slider-on-deck $[Cu_3(\mathbf{1})(\mathbf{2})]^{3+}$ was achieved. Full reversibility of the interconversions over six cycles was proven by alternately adding Pd^{2+} and then DMAP by ^{1}H NMR (ESI, Fig. S12†).
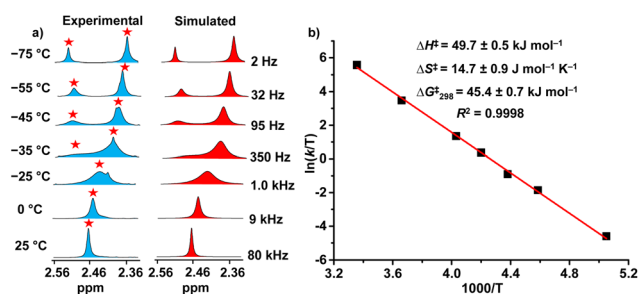

Fig. 2 Comparison of ^{1}H NMR spectra (400 MHz, CD$_2$Cl$_2$: CD$_3$CN = 4 : 1, 298 K) of (a) the slider-on-deck **DS** = $[Cu_3(\mathbf{1})(\mathbf{2})]^{3+}$; (b) **D** = $[Cu_3(\mathbf{1})]^{3+}$ + **C** = $[Pd_2(\mathbf{2})_4]^{4+}$; (c) pentacene-6,13-dione (**G**); (d) NetState-I; (e) NetState-II; (f) cage + pentacene-6,13-dione (1 : 1.5 equivalent) = G@C + G.

Encapsulation of pentacene-6,13-dione (**G**) into the cage **C** = $[Pd_2(\mathbf{2})_4](BF_4)_4$ was realized in CD$_2$Cl$_2$: CD$_3$CN = 4 : 1, similar to the procedure by Lusby[9] *et al.* To achieve complete encapsulation, excess of **G** was required as shown in the UV-vis titration (peaks corresponding to cage **C** at 231, 243, 286, and 301 nm increased gradually saturating upon the addition of 1.5 equiv. of **G**, see Fig. 3a). Therefrom, the binding constant was determined as $\log K = 7.91 \pm 0.29$ (ESI, Fig. S29†). The encapsulation of **G** was also noted from drastic ^{1}H NMR shifts, *e.g.*, proton c′-H, of **C** shifted from 8.03 to 5.48 ppm and proton 1′-H of **G** shifted from 8.91 to 10.06 ppm. Parallel, the

Fig. 1 (a) Partial ^{1}H VT NMR (CD$_2$Cl$_2$, 600 MHz) of the slider-on-deck **DS** shows the splitting of the 3-H proton signal upon lowering the temperature (red asterisk). (b) Eyring plot for rotational exchange in **DS**.
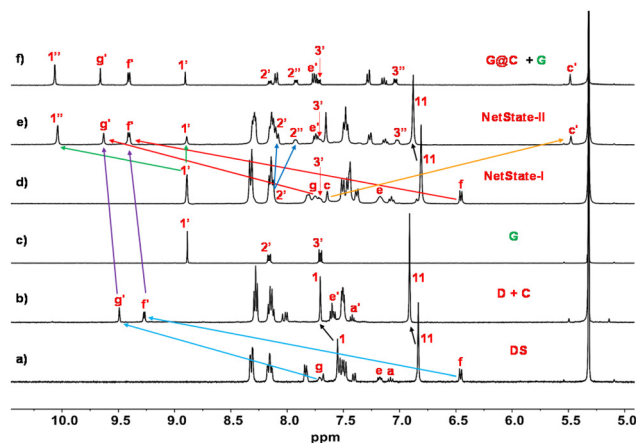
Within Fig. 1b: $\Delta H^{\ddagger} = 49.7 \pm 0.5$ kJ mol^{-1}; $\Delta S^{\ddagger} = 14.7 \pm 0.9$ J mol^{-1} K^{-1}; $\Delta G^{\ddagger}_{298} = 45.4 \pm 0.7$ kJ mol^{-1}; $R^2 = 0.9998$
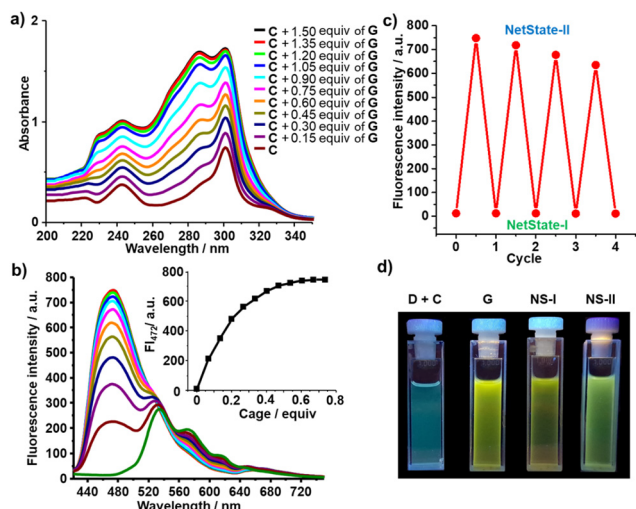

Fig. 3 (a) UV–vis titration of the cage (**C**) (1.56 μM) with pentacene-6,13-dione (**G**); (b) fluorescence titration of guest **G** (1.75 μM) with cage **C**; (c) reversible switching between NetState-I and II in presence of Pd^{2+} and DMAP over four cycles monitored by fluorescence intensity at $\lambda = 472$ nm; (d) **D** + **C**, free **G**, and NetState-II under a 365 nm UV lamp (from left to right).

ESI-MS proved guest encapsulation into the cage by peaks at m/z = 411.0 (quadruply charged), m/z = 576.1 (triply charged), and m/z = 908.0 (doubly charged) (ESI, Fig. S28†). Cross-correlations between proton c′-H of the cage and protons 1″-H, 2″-H, and 3″-H of **G** in the ^{1}H–^{1}H NOESY spectrum attested to the formation of the host–guest system (ESI, Fig. S13†). In fluorescence spectroscopy, the addition of the cage to the ligand showed a blue shift (Fig. 3b). Initially, the emission of **G** (excited at λ = 300 nm) revealed a bright yellow fluorescence at λ = 537 and 569 nm. In the ensuing titration with **C**, the initial peaks of **G** gradually disappeared, while simultaneously a new strong emission at λ = 472 nm emerged showing as a bright green fluorescence.

To afford NetState-I = **DS** + **G**, deck **1**, biped **2**, [Cu(CH$_3$CN)$_4$]PF$_6$, and **G** were mixed (1 : 1 : 3 : 1.5). After the clean formation of NetState-I, 0.5 equiv. of [Pd(CH$_3$CN)$_4$](BF$_4$)$_2$ was added which resulted in the formation of NetState-II = **D** + **G@C** + **G**. The binding constant of **G@C** in NetState-II was identical to that of the isolated system (ESI, Fig. S29b & S30†). The Pd(II) coordination to biped **2** happened quite rapidly ($t_{\frac{1}{2}}$ = 26.5 ± 0.9 s) even at low concentration (c = 1.22 × 10^{-6} M) as used in a UV-Vis kinetic study (ESI, Fig. S37†). Equally in the reverse translocation of NetState-II to NetState-I, dissolution of cage **G** and coordination of Pd(II) to DMAP was rapid ($t_{\frac{1}{2}}$ = 56.5 ± 1.4 s at c = 1.22 × 10^{-6} M; ESI, Fig. S38†). Both multi-component assemblies were identified by ^{1}H-NMR (Fig. 2). Since there is no ^{1}H-NMR peak shift in NetState-I regarding the separate entities, apparently there is no interaction between **G** and **DS**. In NetState-II though, the peaks of proton c-H of the **DS** and 1′-H of the **G** were shifted from 7.68 and 8.91 ppm to 5.49 and 10.06 ppm, respectively, due to cage formation along with guest encapsulation. In this regard, the shift of the proton signals f′-H and g′-H from 9.34 and 9.50 ppm (free **C**) to 9.42 and 9.66 ppm (after encapsulation of **G**), respectively, was diagnostic.

Reversibility of the networked system upon alternate addition of Pd^{2+} and DMAP over four cycles was established by ^{1}H NMR (Fig. 4). The interconversion of NetState-I ⇄ NetState-II was conveniently followed by fluorescence because the yellow emission of free **G** shifted to green after encapsulation of **G**. Upon addition of DMAP, the emission reversed to the initial wavelength. Changes between the two states were reproduced over four cycles (Fig. 3c) with a small decline in the emission intensity, most likely due to the formation of [Pd(DMAP)$_4$]$^{2+}$.

The catalytic cyclization of **4** to isoquinolinium imide **5** is known for Ag$^+$,[16] Fe^{3+},[17] I$_2$, Br$_2$, I–Cl, NIS, NBS,[18] and for Cu^{2+} ions.[19] In the present work, we achieved cyclization with Cu$^+$ ions (Scheme 2). The cyclization of **4** (c = 3.38 mM) was first studied in presence of [Cu(CH$_3$CN)$_4$]PF$_6$ (15 mol%) at 40 °C in CD$_2$Cl$_2$: CD$_3$CN = 4 : 1 yielding 20 (±2)% of **5** after 7 h (ESI, Fig. S24†). Due to the facile oxidation of free [Cu(CH$_3$CN)$_4$]PF$_6$ to copper(II), performing the second cycle of the reaction and simultaneously monitoring by ^{1}H NMR was not achievable. In contrast, copper(I) in [Cu$_3$(**1**)]$^{3+}$ and [Cu$_3$(**1**)(**2**)]$^{3+}$ should be stabilized against oxidation because of coordination with the
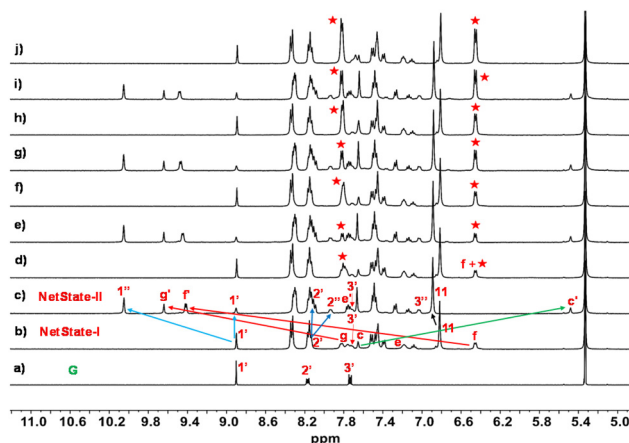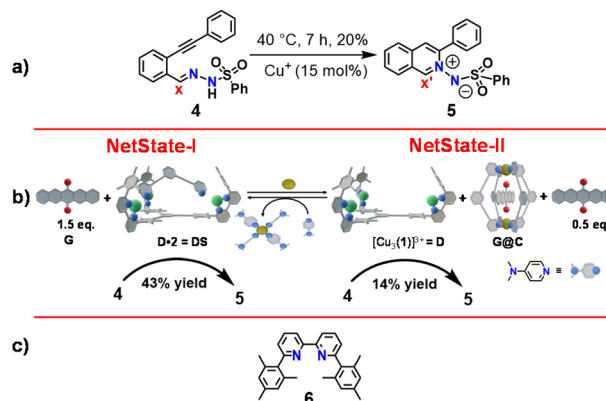

Fig. 4 Reversibility of the NetState-I and II in the presence of Pd^{2+} and DMAP over four cycles monitored by ^{1}H NMR (400 MHz, CD$_2$Cl$_2$: CD$_3$CN (4 : 1), 298 K). (a) **G**; (b) NetState-I; (c) NetState-II; (d) NetState-I; (e) NetState-II; (f) NetState-I; (g) NetState-II; (h) NetState-I; (i) NetState-II; (j) NetState-I. The red star indicates peaks of [Pd(DMAP)$_4$]$^{2+}$.

Scheme 2 (a) Schematic presentation of the catalysis reaction used in this work. (b) Yield of cyclization reaction in presence of 5 mol% of both NetStates in CD$_2$Cl$_2$: CD$_3$CN (4 : 1) at 40 °C for 7 h. (c) Ligand **6**, which is used in species distribution experiments.

stator's bipyridine. As a result, we expected copper(I) to be catalytically active in the NetState-I/II system over multiple switching cycles and performed three reversible catalytic cycles (c = 3.38 mM, in CD$_2$Cl$_2$: CD$_3$CN = 4 : 1, at 40 °C, 7 h) alternatingly adding Pd^{2+} and DMAP (ESI, Fig. S19†). As determined by ^{1}H NMR, the yield of product **5** was (43 ± 2)% in NetState-I and (14 ± 2)% in state-II, being reproducible over all three cycles (Scheme 2b and ESI, Fig. S20†). To exclude the possible involvement of Pd^{2+} as a catalyst, we tested the reaction of **4** (in CD$_2$Cl$_2$: CD$_3$CN = 4 : 1 at 40 °C for 7 h) in the presence of either [Pd(DMAP)$_4$]$^{2+}$ or cage. Neither cage, free palladium ions nor [Pd(DMAP)$_4$]$^{2+}$ were active as catalysts (ESI, Fig. S21–23†).

Although the higher yields in NetState-I $vs.$ II are counterintuitive at first, the difference was expected based on previous

studies.[20] As outlined there,[20] the motion in the slider-on-deck may reduce binding of **5** to copper(I) and thus product inhibition of **DS** as catalyst. Indeed, investigations show that 83% of **5** was liberated into solution from $[Cu_3(\mathbf{1})(\mathbf{2})(\mathbf{5})]^{3+}$ due to the sliding motion (ESI,† pages S33–35), whereas in a static reference, *i.e.*, complex $[Cu(\mathbf{6})(\mathbf{5})]^+$ representing **D** as catalyst, only 58% of **5** are freed (ESI, Fig. S35†).

In conclusion, we demonstrated a functional network, in which copper(I) catalysis was highly reproducibly up/down regulated by removal/addition of Pd^{2+}. Parallel, the encapsulation of 6,13-pentacendione[9] as a guest in NetState-II provided diagnostic on/off emission changes reporting the interconversion of the networked states. Fully reversible interconversion between NetState-I and II was realized by the addition of stoichiometric amounts of Pd^{2+} and DMAP over four cycles in the case of encapsulation and three in the case of catalysis. The present work demonstrates how new functions (catalysis with parallel fluorescence signalling) emerge from networked systems.

Author contributions

Isa Valiyev: conceptualization, investigation, writing – original draft. Indrajit Paul: investigation. Yi-Fan Li: investigation. Emad Elramadi: investigation. Michael Schmittel: project administration, funding acquisition, supervision, writing – review & editing.

Conflicts of interest

There are no conflicts to declare.

Acknowledgements

References

1 P. Neupane, S. Bhuju, N. Thapa and H. K. Bhattarai, *Biomol. Concepts*, 2019, **10**, 1–10, DOI: **10.1515/bmc-2019-0001**.

2 (*a*) R. L. Spicer, A. D. Stergiou, T. A. Young, F. Duarte, M. D. Symes and P. J. Lusby, *J. Am. Chem. Soc.*, 2020, **142**, 2134–2139, DOI: **10.1021/jacs.9b11273**; (*b*) J. Tessarolo, H. Lee, E. Sakuda, K. Umakoshi and G. H. Clever, *J. Am. Chem. Soc.*, 2021, **143**(17), 6339–6344, DOI: **10.1021/jacs.1c01931**; (*c*) L. Escobar and P. Ballester, *Chem. Rev.*, 2021, **121**, 2445–2514, DOI: **10.1021/acs.chemrev.0c00522**; (*d*) R. Saha, B. Mondal and P. S. Mukherjee, *Chem. Rev.*, 2022, **122**, 12244–12307, DOI: **10.1021/acs.chem-rev.1c00811**; (*e*) L. S. Lisboa, M. Riisom, H. J. Dunne, D. Preston, S. M. F. Jamieson, L. J. Wright, C. G. Hartinger and J. D. Crowley, *Dalton Trans.*, 2022, **51**, 18438–18445, DOI: **10.1039/D2DT02720H**; (*f*) R.-J. Li, J. de Montmollin, F. Fadaei-Tirani, R. Scopelliti and K. Severin, *Dalton Trans.*, 2023, **52**, 6451–6456, DOI: **10.1039/D3DT00248A**.

3 (*a*) H. Ube, R. Yamada, J.-I. Ishida, H. Sato, M. Shiro and M. Shionoya, *J. Am. Chem. Soc.*, 2017, **139**, 16470–16473, DOI: **10.1021/jacs.7b09439**; (*b*) N. Mittal, S. Pramanik, I. Paul, S. De and M. Schmittel, *J. Am. Chem. Soc.*, 2017, **139**, 4270–4273, DOI: **10.1021/jacs.6b12951**; (*c*) P. K. Biswas, S. Saha, Y. Nanaji, A. Rana and M. Schmittel, *Inorg. Chem.*, 2017, **56**, 6662–6670, DOI: **10.1021/acs.inorgchem.7b00740**; (*d*) A. Goswami, S. Saha, P. K. Biswas and M. Schmittel, *Chem. Rev.*, 2020, **120**(1), 125–199, DOI: **10.1021/acs.chemrev.9b00159**.

4 (*a*) I. Paul, A. Goswami, N. Mittal and M. Schmittel, *Angew. Chem., Int. Ed.*, 2018, **57**, 354–358, DOI: **10.1002/anie.201709644**; (*b*) S. Kundu, I. Valiyev, D. Mondal, V. V. Rajasekaran, A. Goswami and M. Schmittel, *RSC Adv.*, 2023, **13**, 5168–5171, DOI: **10.1039/d3ra00062a**; (*c*) E. Elramadi, S. Kundu, D. Mondal and M. Schmittel, *Chem. Commun.*, 2023, **59**, 4915–4918, DOI: **10.1039/d3cc00637a**.

5 (*a*) L. van Dijk, M. J. Tilby, R. Szpera, O. A. Smith, H. A. P. Bunce and S. P. Fletcher, *Nat. Rev. Chem.*, 2018, **2**, 117, DOI: **10.1038/s41570-018-0117**; (*b*) A. Goswami, T. Paululat and M. Schmittel, *J. Am. Chem. Soc.*, 2019, **141**, 15656–15663, DOI: **10.1021/jacs.9b07737**.

6 (*a*) L.-J. Chen, H.-B. Yang and M. Shionoya, *Chem. Soc. Rev.*, 2017, **46**, 2555–2576, DOI: **10.1039/c7cs00173h**; (*b*) M. Pan, K. Wu, J.-H. Zhang and C.-Y. Su, *Coord. Chem. Rev.*, 2019, **378**, 333–349, DOI: **10.1016/j.ccr.2017.10.031**.

7 (*a*) T. M. Bräuer, Q. Zhang and K. Tiefenbacher, *J. Am. Chem. Soc.*, 2017, **139**, 17500–17507, DOI: **10.1021/jacs.7b08976**; (*b*) Y. Zhu, J. Rebek Jr. and Y. Yu, *Chem. Commun.*, 2019, **55**, 3573–3577, DOI: **10.1039/c9cc01611b**; (*c*) Y. Peng, Z. Su, M. Jin, L. Zhu, Z.-J. Guan and Y. Fang, *Dalton Trans.*, 2023, **52**, 15216–15232, DOI: **10.1039/D3DT01679J**.

8 (*a*) A. C. H. Jans, A. Gómez-Suárez, S. P. Nolan and J. N. H. Reek, *Chem. – Eur. J.*, 2016, **22**, 14836–14839, DOI: **10.1002/chem.201603162**; (*b*) Q. Zhang, L. Catti and K. Tiefenbacher, *Acc. Chem. Res.*, 2018, **51**, 2107–2114, DOI: **10.1021/acs.accounts.8b00320**.

9 D. P. August, G. S. Nichol and P. J. Lusby, *Angew. Chem., Int. Ed.*, 2016, **55**, 15022–15026, DOI: **10.1002/anie.201608229**.

10 (*a*) A. Ghosh, I. Paul, S. Saha, T. Paululat and M. Schmittel, *Org. Lett.*, 2018, **20**, 7973–7976, DOI: **10.1021/acs.orglett.8b03541**; (*b*) S. Saha, P. K. Biswas, I. Paul and M. Schmittel, *Chem. Commun.*, 2019, **55**, 14733–14736, DOI: **10.1039/c9cc07415e**.

11 (*a*) Q. Zhang and K. Tiefenbacher, *Nat. Chem.*, 2015, **7**, 197–202, DOI: **10.1038/nchem.2181**; (*b*) Q. Zhang and K. Tiefenbacher, *Angew. Chem., Int. Ed.*, 2019, **58**, 12688–12695, DOI: **10.1002/anie.201906753**.

12 P. Liao, B. W. Langloss, A. M. Johnson, E. R. Knudsen, F. S. Tham, R. R. Juliana and R. J. Hooley, *Chem. Commun.*, 2010, **46**, 4932–4934, DOI: **10.1039/c0cc00234h**.

13 M. Schmittel, C. Michel, S.-X. Liu, D. Schildbach and D. Fenske, *Eur. J. Inorg. Chem.*, 2001, 1155–1166, DOI: **10.1002/1099-0682(200105)2001:5<1155::AID-EJIC1155>3.0. CO;2-C**.

14 S. Mandal and A. Basak, *Tetrahedron Lett.*, 2009, 3641–3644, DOI: **10.1016/j.tetlet.2009.03.168**.

15 H. J. Reich, *NMR Spectrum Calculations: WinDNMR, Version 7.1.13*, Department of Chemistry, University of Wisconsin.

16 X. Cheng, X. Cao, J. Xuan and W.-J. Xiao, *Org. Lett.*, 2018, **20**, 52–55, DOI: **10.1021/acs.orglett.7b03344**.

17 H.-F. Yao, D.-L. Wang, F.-H. Li, B. Wu, Z.-J. Cai and S.-J. Ji, *Org. Biomol. Chem.*, 2020, **18**, 7577–7584, DOI: **10.1039/d0ob01517b**.

18 Q. Dinga and J. Wu, *Adv. Synth. Catal.*, 2008, **350**, 1850–1854, DOI: **10.1002/adsc.200800301**.

19 J. Chen, B. Liu, Y. Chen, Q. He and C. Yang, *RSC Adv.*, 2014, **4**, 11168–11175, DOI: **10.1039/c3ra47324d**.

20 P. K. Biswas, S. Saha, T. Paululat and M. Schmittel, *J. Am. Chem. Soc.*, 2018, **140**, 9038–9041, DOI: **10.1021/jacs.8b04437**.